Calibration of dynamic holographic optical tweezers for force measurements on biomaterials

Astrid van der Horst and Nancy R. Forde

Department of Physics, Simon Fraser University, 8888 University Drive, Burnaby, BC, V5A 1S6, Canada

astrid.van.der.horst@sfu.ca

nforde@sfu.ca

http://www.sfu.ca/fordelab/

Abstract: Holographic optical tweezers (HOTs) enable the manipulation of multiple traps independently in three dimensions in real time. Application of this technique to force measurements requires calibration of trap stiffness and its position dependence. Here, we determine the trap stiffness of HOTs as they are steered in two dimensions. To do this, we trap a single particle in a multiple-trap configuration and analyze the power spectrum of the laser deflection on a position-sensitive photodiode. With this method, the relative trap strengths can be determined independent of exact particle size, and high stiffnesses can be probed because of the high bandwidth of the photodiode. We find a trap stiffness for each of three HOT traps of $\kappa \sim 26$ pN/μm per 100 mW of laser power. Importantly, we find that this stiffness remains constant within $\pm$ 4% over 20μm displacements of a trap. We also investigate the minimum step size achievable when steering a trap with HOTs, and find that traps can be stepped and detected within $\sim$2 nm in our instrument, although there is an underlying position modulation of the traps of comparable scale that arises from SLM addressing. The independence of trap stiffness on steering angle over wide ranges and the nanometer positioning accuracy of HOTs demonstrate the applicability of this technique to quantitative study of force response of extended biomaterials such as cells or elastomeric protein networks.

OCIS codes: (140.7010) Laser trapping; (170.4520) Optical confinement and manipulation; (230.6120) Spatial light modulators; (350.4855) Optical tweezers.

References and links

1. A. Ashkin, J. M. Dziedzic, J. E. Bjorkholm, and S. Chu, "Observation of a single-beam gradient force optical trap for dielectric particles," Opt. Lett. **11,** 288–290 (1986).
2. J. R. Moffitt, Y. R. Chemla, S. B. Smith, and C. Bustamante, "Recent advances in optical tweezers," Annu. Rev. Biochem. **77**, 205–228 (2008).
3. W. J. Greenleaf, M. T. Woodside, and S. M. Block, "High-resolution, single-molecule measurements of biomolecular motion," Annu. Rev. Biophys. Biomol. Struct. **36**, 171–190 (2007).
4. C. Bustamante, Y. R. Chemla, N. R. Forde, and D. Izhaky, "Mechanical processes in biochemistry," Annu. Rev. Biochem. **73**, 705–748 (2004).
5. G. Lenormand, S. Hénon, A. Richert, J. Siméon, and F. Gallet, "Direct measurement of the area expansion and shear moduli of the human red blood cell membrane skeleton," Biophys. J. **81**, 43–56 (2001).

#103154 - $15.00 USD Received 23 Oct 2008; revised 27 Nov 2008; accepted 28 Nov 2008; published 3 Dec 2008

6. K. Visscher, G. J. Brakenhoff, and J. J. Krol, "Micromanipulation by multiple optical traps created by a single fast scanning trap integrated with the bilateral confocal scanning laser microscope," Cytometry **14**, 105–114 (1993).
7. D. L. J. Vossen, A. van der Horst, M. Dogterom, and A. van Blaaderen, "Optical tweezers and confocal microscopy for simultaneous three-dimensional manipulation and imaging in concentrated colloidal dispersions," Rev. Sci. Instrum. **75**, 2960–2970 (2004).
8. Y. Deng, J. Bechhoefer, and N.R. Forde, "Brownian motion in a modulated optical trap," J. Opt. A: Pure Appl. Opt. **9**, S256–S263 (2007).
9. E. R. Dufresne and D. G. Grier, "Optical tweezer arrays and optical substrates created with diffractive optics," Rev. Sci. Instrum. **69**, 1974–1977 (1998).
10. M. Reicherter, T. Haist, E. U. Wagemann, H. J. Tiziani, "Optical particle trapping with computer-generated holograms written on a liquid-crystal display," Opt. Lett. **24**, 608–610 (1999).
11. L. B. Lesem, P. M. Hirsch, and J. A. Jordan, Jr., "The Kinoform: A New Wavefront Reconstruction Device," IBM J. Res. Dev. **13**, 150–155 (1969).
12. J. Liesener, M. Reicherter, T. Haist, H. J. Tiziani, "Multi-functional optical tweezers using computer-generated holograms," Opt. Commun. **185**, 77–82 (2000).
13. J. E. Curtis, B. A. Koss, and D. G. Grier, "Dynamic holographic optical tweezers," Opt. Commun. **207**, 169–175 (2002).
14. K. D. Wulff, D. G. Cole, R. L. Clark, R. Di Leonardo, J. Leach, J. Cooper, G. Gibson, and M. J. Padgett, "Aberration correction in holographic optical tweezers," Opt. Express **14**, 4169–4174 (2006).
15. G. C. Spalding, J. Courtial, and R. Di Leonardo, "Holographic optical tweezers," in *Structured Light and Its Applications*, D. L. Andrews, ed. (Academic Press, 2008) pp. 139–168.
16. D. G. Grier, "A revolution in optical manipulation," Nature **424**, 810–816 (2003).
17. K. Dholakia, G. Spalding, and M. MacDonald, "Optical tweezers: the next generation," Phys. World **15**, 31–35 (2002).
18. K. C. Neuman and S. M. Block, "Optical trapping," Rev. Sci. Instrum. **75**, 2787–2809 (2004).
19. F. Belloni, S. Monneret, F. Monduc, and M. Scordia, "Multiple holographic optical tweezers parallel calibration with optical potential well characterization," Opt. Express **16**, 9011–9020 (2008).
20. G. Sinclair, P. Jordan, J. Leach, M. J. Padgett, and J. Cooper, "Defining the trapping limits of holographical optical tweezers," J. Mod. Opt. **51**, 409–414 (2004).
21. R. Di Leonardo, F. Ianni, G. Ruocco, "Computer generation of optimal holograms for optical trap arrays," Opt. Express **15**, 1913–1922 (2007).
22. E. Hällstig, L. Sjöqvist, and M. Lindgren, "Intensity variations using a quantized spatial light modulator for nonmechanical beam steering," Opt. Eng. **42**, 613–619 (2003).
23. K. L. Tan, S. T. Warr, I. G. Manolis, T. D. Wilkinson, M. M. Redmond, W. A. Crossland, R. J. Mears, and B. Robertson, "Dynamic holography for optical interconnections. II. Routing holograms with predictable location and intensity of each diffraction order," J. Opt. Soc. Am. A **18**, 205–215 (2001).
24. D. R. Burnham and D. McGloin, "Holographic optical trapping of aerosol droplets," Opt. Express **14**, 4175–4181 (2006).
25. B. C. Carter, G. T. Shubeita, and S. P. Gross, "Tracking single particles: a user-friendly quantitative evaluation," Phys. Biol. **2**, 60–72 (2005).
26. K. Visscher, S. P. Gross, and S. M. Block, "Construction of multiple-beam optical traps with nanometer-resolution position sensing," IEEE J. Sel. Top. Quantum Electron. **2**, 1066–1076 (1996).
27. K. Berg-Sørensen and H. Flyvbjerg, "Power spectrum analysis for optical tweezers," Rev. Sci. Instrum. **75**, 594–612 (2004).
28. M. Polin, K. Ladavac, S.-H. Lee, Y. Roichman, and D. G. Grier, "Optimized holographic optical traps," Opt. Express **13**, 5831–5845 (2005).
29. S. Keen, J. Leach, G. Gibson, and M. Padgett, "Comparison of a high-speed camera and a quadrant detector for measuring displacements in optical tweezers," J. Opt. A: Pure Appl. Opt. **9**, S264–S266 (2007).
30. M. W. Allersma, F. Gittes, M. J. deCastro, R. J. Stewart, and C. F. Schmidt, "Two-dimensional tracking of ncd motility by back focal plane interferometry," Biophys. J. **74**, 1074–1085 (1998).
31. S. Osten, S. Krüger, and A. Hermerschmidt, "New HDTV (1920×1080) phase-only SLM," Proc. SPIE **6487**, 64870X (2007).
32. U. Klug, M. Boyle, F. Friederich, R. Kling, and A. Ostendorf, "Laser beam shaping for micromaterial processing using a liquid crystal display," Proc. SPIE **6882**, 688207 (2008).
33. S. Serati and J. Harriman, "Spatial light modulator considerations for beam control in optical manipulation applications," Proc. SPIE **6326**, 63262W (2006).
34. J. E. Curtis, C. H. J. Schmitz, and J. P. Spatz, "Symmetry dependence of holograms for optical trapping," Opt. Lett. **30**, 2086–2088 (2005).
35. C. H. J. Schmitz, J. P. Spatz, and J. E. Curtis, "High-precision steering of multiple holographic optical traps," Opt. Express **13**, 8678–8685 (2005).
36. E. Eriksson, S. Keen, J. Leach, M. Goksör, and M. J. Padgett, "The effect of external forces on discrete motion within holographic optical tweezers," Opt. Express **15**, 18268–18274 (2007).

#103154 - $15.00 USD Received 23 Oct 2008; revised 27 Nov 2008; accepted 28 Nov 2008; published 3 Dec 2008

37. M. T. Valentine, N. R. Guydosh, B. Gutiérrez-Medina, A. N. Fehr, J. O. Andreasson, and S. M. Block, "Precision steering of an optical trap by electro-optic deflection," Opt. Lett. **33**, 599–601 (2008).
38. A. Pralle, M. Prummer, E.-L. Florin, E. H. K. Stelzer, and J. K. H. Hörber, "Three-dimensional high-resolution particle tracking for optical tweezers by forward scattered light," Microsc. Res. Tech. **44**, 378–386 (1999).
39. S.-H. Lee, Y. Roichman, G.-R. Yi, S.-H. Kim, S.-M. Yang, A. van Blaaderen, P. van Oostrum, and D. G. Grier, "Characterizing and tracking single colloidal particles with video holographic microscopy," Opt. Express **15**, 18275–18282 (2007).

1. Introduction

In recent years, optical tweezers [1] have emerged as a leading technique in the field of biophysics, due to their ability to constrain the position of micrometer-sized objects in three dimensions and to detect and exert biologically relevant picoNewton forces. Optical tweezers have found a particularly fruitful application to single-molecule studies, where tethering macromolecules to optically trapped beads has enabled measurements of their response to extension and force, revealing, *e.g.*, mechanical response properties of DNA and free energy surfaces for nucleic acid and protein unfolding [2–4].

Extending the manipulation and force measurement capabilities of optical tweezers to the mechanical probing of higher-order biological structures, such as cells and soft biomaterials, requires the ability to stretch these higher-dimensional structures in more than one direction. This has been accomplished for example using 'time-sharing' to trap multiple microspheres bound to a red blood cell [5]. With time-sharing [6], steerable mirrors or acousto-optic deflectors are used to rapidly scan the laser beam among multiple locations and thus trap many objects simultaneously [7]. However, the quantitative interpretation of measured forces relies on the ability to scan the laser among locations much faster than the characteristic response time of the trapped object + material [6, 8]; a time that is not known *a priori*, and which, especially for stiffer biomaterials, may be significantly faster than accessible steering speeds.

An alternative method of creating multiple optical traps is holographic optical tweezers (HOTs) [9, 10]. In this technique, the laser beam is sent through or reflected off a so-called kinoform [11], a spatial pattern of local phase retardations that changes the wavefront of the laser beam. The modulation of the phase is transformed into a modulation of light intensity by focusing through a microscope objective lens. Thus, by choosing a certain kinoform, multiple focal spots can be created. Dynamic modulation of the phase can be accomplished by use of a spatial light modulator (SLM) in which the kinoform can be changed in real time. The use of an SLM in HOTs [12, 13] allows for the individual dynamic steering of multiple optical traps. With this technique, the position in the third dimension (along the optical axis) can be controlled for each trap individually, a distinct advantage over other beam steering approaches. In addition, the SLM can be used to compensate for aberrations in the optical system [14]. The beam-shaping and -steering characteristics afforded by dynamic HOTs have been widely exploited within the physics community [15–17]. However, the technique of HOTs has not yet found widespread application in biophysics, in large part due to lack of evidence as to how forces exerted by holographic optical traps vary as the phase of the beam is modulated.

Force measurements require calibrated traps, *i.e.*, knowledge of the trap stiffness κ, the relationship between the displacement Δx of a particle from its equilibrium position and the force F exerted on the particle ($\kappa = -F / \Delta x$). Calibration of κ is straightforward and well established for single optical traps [18]. Studies to date on HOTs, however, have found sharp declines in trap stiffness and trapping efficiency as traps are steered further from their zero-order (unmodulated) direction [19, 20].

Here, we systematically characterize traps within HOTs as they are steered in two-dimensional configurations relevant for studies of soft biomaterials. We first examine the temporal stability of trap position and intensity for HOTs. We then address the question of how

#103154 - $15.00 USD Received 23 Oct 2008; revised 27 Nov 2008; accepted 28 Nov 2008; published 3 Dec 2008

much the average stiffness of an optical trap changes when it is steered, or when it is stationary but another trap within the HOTs is steered. By steering our traps over distances small and large, we determine the range over which the trap stiffness remains constant. We compare the results of our measurements to theoretical predictions and find reasonable agreement. We also determine the efficiency of diffraction into the first-order steered traps compared to the zero-order spot, and we find a linear dependence of trap stiffness on laser power, as expected. Finally, we determine the smallest detectable step size for beam steering in our HOT instrument.

2. Theory

In this section, we outline a simple, analytical description of steering an optical trap using a phase-only spatial light modulator, such as a reflective phase-only liquid-crystal SLM (LC-SLM), in which the LC orientation within each pixel (set by the user) determines the phase retardation imposed on the light traveling through that pixel. We use this model to demonstrate how the characteristics of the SLM (dimensions, phase retardation, etc.) relate to the displacement of an optical trap in a sample chamber and how the diffraction efficiency is expected to change as the trap is steered further from the zero-order (undiffracted) peak.

2.1. SLM beam steering – phase modulation by kinoforms

One of the most straightforward phase modulations is the phase gradient. Similar to the phase changes introduced by tilting a mirror, a kinoform with a linear phase delay gradient will change the angle α of the refracted laser beam (Fig. 1). With the SLM reimaged onto the back focal plane (BFP) of an objective lens, this change in angle results in a displacement d of the focal spot in the front focal plane (FFP). To steer the focal spot in two dimensions, a phase gradient in both x and y is chosen for the kinoform. To create multiple optical traps, *i.e.* multiple foci, the complex sum of the kinoforms for each of the desired trap positions is taken. This scheme [11, 12] is implemented to create the kinoforms used in the experiments described in this paper. Alternative methods of phase modulation for beam steering exist [21], but are not investigated here.

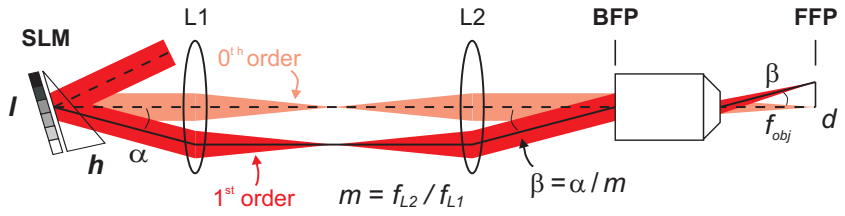

Fig. 1. Schematic depiction of SLM beam steering. A laser beam is reflected off the SLM. A phase gradient proportional to h/l steers the beam by an angle α. Lenses $L1$ and $L2$ (in 4f-configuration) image the SLM onto the back focal plane (BFP) of the objective lens with magnification m, the ratio of the focal lengths of lenses $L2$ and $L1$. The unmodulated light (0^{th} order) is focused on the optical axis. The modulated beam (1^{st} order) enters the objective under an angle $\beta=\alpha/m$. In the front focal plane (FFP) this beam is focused at a position displaced d from the zero-order peak. The dependence of d on parameters of the optical system is given by Eq. (3). This schematic is not to scale, and the phase of the laser is modulated over the entire width l of our SLM.

#103154 - $15.00 USD Received 23 Oct 2008; revised 27 Nov 2008; accepted 28 Nov 2008; published 3 Dec 2008

2.2. *Trap displacement* d *as a function of phase gradient*

The way in which the displacement d of the focal spot in the FFP relates to the steering angle α of the first-order beam depends on many parameters of the experimental configuration. For simple small-angle gradient steering (Fig. 1), d relates to α as:

$$\alpha \approx \frac{h}{l} = m\frac{d}{f_{obj}}. \tag{1}$$

Here, the phase gradient is proportional to h/l, where h is the maximum retardation of the optical path measured in meters, and l is the width of the SLM, equal to the product of the number of pixels over which modulation occurs and the pixel pitch l_{pix}. The focal length of the objective is $f_{obj} = L/M$, in which L is the tube length or reference focal length of the objective lens and M is its magnification. The magnification m is the ratio of the focal lengths of lenses *L2* and *L1* in 4f-configuration.

The maximum retardation h can be determined from the maximum imposed phase shift ϕ, and the wavelength of the modulated light λ:

$$h = \frac{\phi}{2\pi}\lambda. \tag{2}$$

So we find for the displacement of the laser trap d in the focal plane:

$$d = \frac{1}{m}\frac{L}{M}\frac{\lambda}{l}\frac{\phi}{2\pi}. \tag{3}$$

As can be seen from Eq. (1), a large displacement of the trap per steering angle α is obtained for a large f_{obj} and a small magnification m.

2.3. *SLM diffraction efficiency*

A phase gradient imposed by an SLM is not ideal. An LC-SLM is pixelated and phase retardation levels are discrete. As a consequence, the first-order diffraction efficiency η of the SLM depends on steering angle α. When this steering is accomplished by a blazed grating (applying $\phi[mod(2\pi)]$) with period Λ (in pixels) and q phase levels, the efficiency η is given by [22, 23]:

$$\eta = \frac{sinc^2(1/q) \times sinc^2(1/\Lambda)}{sinc^2(1/lcm[q,\Lambda])}, \tag{4}$$

where $lcm[q,\Lambda]$ is the least common multiplier of q and Λ. As the beam is steered over larger angles, the phase gradient increases, leading to a blazed grating with smaller Λ and a larger effective discretization of the phase (a decrease in q, even when a large number of phase levels are available on the SLM). This inability of the pixelated SLM to capture the smooth gradient leads to a decreasing efficiency of diffraction into the desired first-order beam. The diffraction efficiency also depends on the fill-factor of the SLM (the ratio of pixel width to pixel pitch), and decreases for larger dead space between pixels [22, 23].

In Fig. 2 the efficiency η is plotted as a function of the normalized angle $\alpha_{norm} = \alpha/\alpha_{max}$, with α_{max} the maximum obtainable deflection angle (obtained with $\Lambda = 2$, a binary π grating). Since $\alpha_{max} = \lambda / 2l_{pix}$ and pixel dimensions are generally much greater than the wavelength of light, even a deflection of α_{max} is a small steering angle of the beam. For our setup, α_{max} = 0.0665 rad (3.8°). Designing a system to have a larger α_{max} (smaller pixel pitch for a given λ) would provide a larger angular range over which the efficiency is roughly constant.

#103154 - $15.00 USD Received 23 Oct 2008; revised 27 Nov 2008; accepted 28 Nov 2008; published 3 Dec 2008

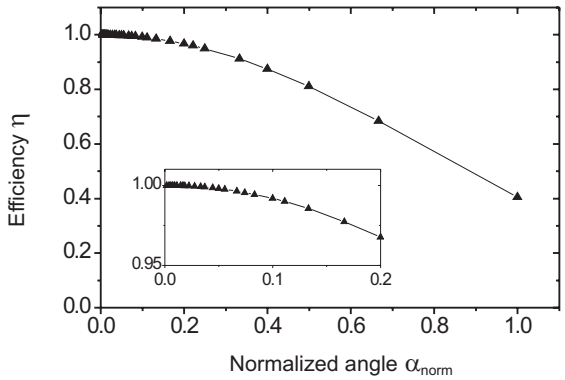

Fig. 2. Theoretical SLM efficiency η due to pixelation and quantization of the phase levels (triangles, Eq. (4)); lines are a guide to the eye. Here, the maximum number of phase levels is taken to be q_{max} = 256, as available on our SLM. For q_{max} = 192 the values are the same (within 0.01%). The normalized angle $\alpha_{norm} = \alpha/\alpha_{max}$, see text. Inset: expanded view of η as a function of α_{norm}. An angle of α_{norm} = 0.2 corresponds to 10 pixels per 2π of phase modulation or, in our setup, d = 39.9 μm.

3. Experimental methods

3.1. Holographic optical tweezers setup

In our holographic optical tweezers setup, the TEM_{00} mode of an infrared (IR) laser (Spectra Physics, J20-BL-106C, 4 Watt CW, 1064 nm) is used for trapping (Fig. 3). After passing through an optical isolator (OFR, O-3-1064-VHP), the beam is expanded by a beam expander (LINOS Photonics, 2–8×) to overfill the short (vertical) axis of an SLM (HoloEye HEO 1080P LCOS phase only, 1920×1080 pixel^2, pixel pitch $l_{pix} = 8\mu$m, refresh rate 60 Hz). A half-lambda zero-order wave plate in combination with a polarizing beam splitter cube provides manual control over the power directed to the SLM. Mirror *M1* reflects the beam onto the SLM, where the angle between the incoming beam and reflected zero-order beam is approximately 8 °. The lenses *L1* and *L2* (each with focal length 250 mm) place the SLM in a plane conjugate to the back focal plane of an infinity-corrected high-numerical aperture (NA) objective (Olympus UplanApo/IR, 60×, 1.2 NA, water immersion, reference focal length L=180 mm). The modulated laser beam slightly overfills the back aperture of this lens. A second, identical objective is used to capture the laser light, and lens *L3* images the back focal plane of this objective onto a position-sensitive diode (PSD; OSI Optoelectronics, DL-10). Dichroic mirrors *D1* and *D2* (Chroma Technology Corp., 900DCSP) enable illumination in the visible (Dolan Jenner, Fiber Lite 180). The signals from the PSD are collected using a home-built amplifier, and are read by a computer using a DAQ board (National Instruments, PCI-6052E).

Two cameras are used to image the trapped particles: a CCD (Point Grey Research, FL2-03S2M) runs continuously at typical video frame rates during operation, while a high-speed CMOS camera (PCO, 1200 hs, 1280×1024 pixels, pixel size $12\times12\mu m^2$) is used for our measurements of particle positions at high bandwidth (>1kHz). The 10-bit high-speed camera images are saved as 8-bit *.tiff* files and are analyzed offline (see subsection 3.2). Our high-speed camera images were calibrated for position detection using a stage micrometer, giving 1 pixel = 53.1 nm. The laser, DAQ board, and standard CCD camera are controlled by one PC, while a second PC is dedicated to the high-speed camera. Kinoforms were calculated in Lab-

#103154 - $15.00 USD Received 23 Oct 2008; revised 27 Nov 2008; accepted 28 Nov 2008; published 3 Dec 2008

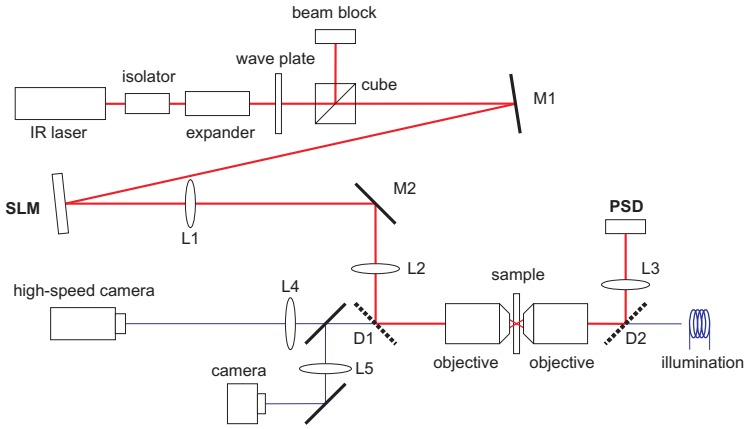

Fig. 3. Schematic of the holographic tweezers setup. A spatial light modulator (SLM) modulates the wavefront of an infrared laser beam. A high-numerical aperture objective focuses the light, and multiple optical traps can be created. A second identical objective captures the light, which is imaged onto a position-sensitive diode (PSD) for particle position detection. Particle imaging uses counterpropagating visible light, with the image directed to two cameras. See text for details.

VIEW [24] and astigmatism in the optical trap focus was reduced by adding to each kinoform a fixed correction kinoform calculated using Zernike polynomials [14]. All stated laser powers are measured between the SLM and the focusing objective lens.

In the work described in this paper, we trapped 2.1-μm-diameter polystyrene spheres (Spherotech) dispersed in water. Our trapping experiments were performed in the middle of sample cells that consisted of two microscope cover slips, with a fluid channel created by melted Nescofilm spacers (NESCO, thickness 100 μm) and sealed at their edges by candle wax.

For our experimental setup, Eq. (3) gives a theoretical displacement d per 2π phase retardation of $d_{2\pi} = 0.369\ \mu$m ($m = 1$, $L = 180$ mm, $M = 60$, $\lambda = 1064$ nm, and the size of the kinoform on the SLM $l = 8.64$ mm).

3.2. Particle position detection from image analysis

A home-written LabVIEW program was used for spatial correlation analysis of the high-speed camera images. The algorithm first determines the correlation matrix of a template image of the particle with the current image [25]. The 7×7 points around the maximum of this matrix are fit with a 2D parabolic function, giving the sub-pixel position of the template.

To determine the accuracy of our position detection method we captured 4000 consecutive images of seven particles fixed to a cover slip. Using our tracking algorithm, we determined the position of each particle with respect to the center of particle mass in each of the frames. Assuming the distance between the particles to be constant, the spread in the measured distances among images is due to the error in position detection. We found the position accuracy to be 0.02 pixel, corresponding to 1 nm (2σ).

3.3. Trap stiffness measurements

Power spectral analysis [26, 27] was used to determine the stiffness of optical traps in these measurements. The power spectrum S_x of the trapped particle's position noise in x as a function

#103154 - $15.00 USD Received 23 Oct 2008; revised 27 Nov 2008; accepted 28 Nov 2008; published 3 Dec 2008

of the frequency f is given by a Lorentzian:

$$S_x = \frac{k_B T}{2\pi^2 \gamma (f_c^2 + f^2)}, \tag{5}$$

in which the theoretical viscous drag coefficient for our spheres in water is γ = 1.98$\times$ 10^{-8} kg/s, f_c is the corner frequency, k_B is the Boltzmann constant, and T is the temperature. The trap stiffness κ is related to f_c through:

$$\kappa = 2\pi\gamma f_c. \tag{6}$$

Power spectral analysis was chosen as it is clear to see how drift and external sources of noise contribute to the motion of the particle. These may be harder to observe with other commonly used techniques such as equipartition analysis and analysis of the distribution of particle positions [18], though can be accounted for when calibrating weak traps [28].

Particle positions obtained from high-speed camera measurements can be used to determine the power spectrum of particles' position noise in optical traps [29], up to the Nyquist frequency of half the camera's bandwidth. This approach enables the simultaneous calibration of multiple traps, as long as the corner frequency of each is well below the Nyquist frequency. Practically, current speeds of downloading images from high-speed cameras limit the application of this approach as a rapid screen for trap stiffness.

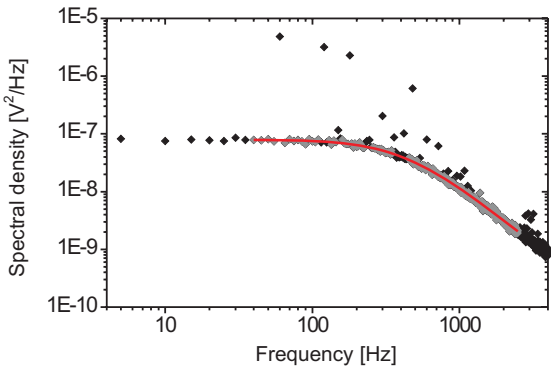

Fig. 4. Example of a measured power spectral density curve (black diamonds), which shows the expected Lorentzian behavior, along with peaks due to the intrinsic SLM address rate. These peaks are deleted prior to analysis, and a Lorentzian (red line) is fit to the spectrum from 40-2500 Hz (grey diamonds) to obtain the corner frequency f_c and thereby the trap stiffness κ (Eqs. (5) and (6)). Here, f_c = 407 Hz and κ = 51 pN/μm.

An alternative and more common method of power spectrum determination analyzes the displacement of the laser light on a PSD [30]. This method is fast in data acquisition and analysis, and is limited only by the frequency response of the photodiode and associated electronics. For a single optical trap, the analysis is straightforward. But if multiple particles are trapped, the laser deflection contains information about the noise of all particles and hence cannot be used in a straightforward manner to determine trap stiffnesses. However, if only one particle is trapped in a multiple-trap configuration, the modulation of the output laser beam is due only to the motion of this single particle. Hence, by trapping only one particle in a HOT configuration, the Lorentzian shape of the power spectrum is due only to the interaction of the single trapped

#103154 - $15.00 USD Received 23 Oct 2008; revised 27 Nov 2008; accepted 28 Nov 2008; published 3 Dec 2008

particle with the trap in which it resides. By moving the same particle from one trap to another, the trap stiffness of each trap can be determined, thus affording a quantitative determination of the relative trap strengths in HOTs independent of exact particle size.

Figure 4 shows a typical power spectrum (averaged over 250 spectra taken over 0.2 s each) arising from one trapped particle held in trap #1 shown in Fig. 7(a). The peaks at discrete frequencies (60 and 120 Hz and overtones) are due to the method used to address the LC of our SLM; this is discussed in section 3.4, below. Because the temporal modulation of the trapping beam by the SLM appears at well defined frequencies, we remove these peaks prior to fitting a Lorentzian to the power spectrum, to determine the average trap stiffness resulting from a given imposed kinoform. The fitting is done to the region $f>40$ Hz to exclude low-frequency noise, and $f<2500$ Hz to exclude artifacts due to aliasing.

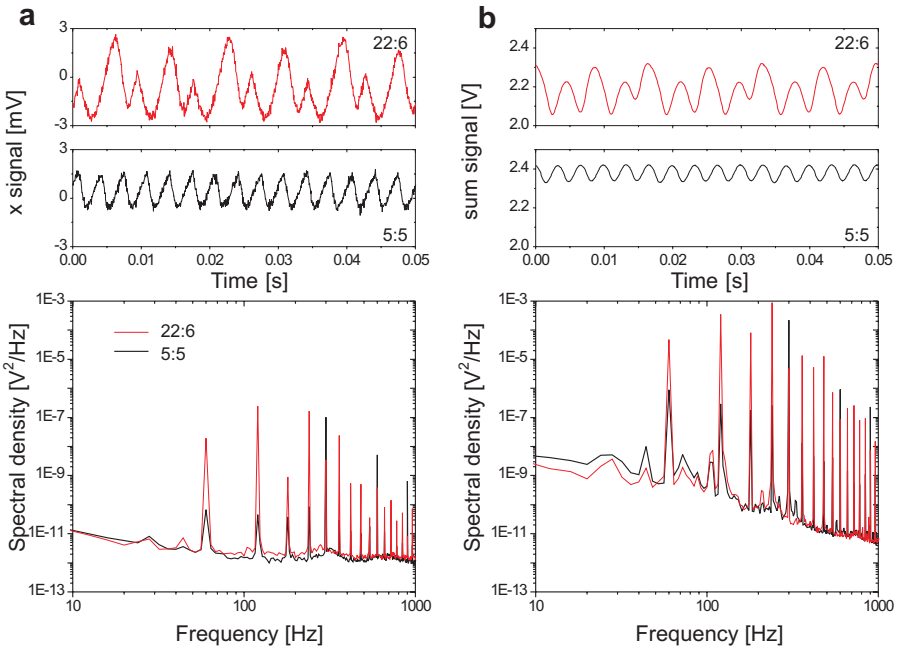

Fig. 5. Displacement in x (a) and intensity (b) as a function of time for a single first-order beam at an angle of α_{norm} = 0.10 in x. These were recorded on our optical table using a PSD by passing only this first-order beam through a small aperture (1 mm diameter) at the conjugate trapping plane between lens L1 and mirror M2. Shown are the data recorded for 22:6 (top) and 5:5 (middle) SLM settings, and power spectra (bottom) for both settings. Laser power was 286 mW.

3.4. Time-dependent modulation of traps due to the SLM

The HoloEye SLM used in our measurements is controlled as an external monitor with a *refresh* rate of 60 Hz. The LC pixels themselves, however, are addressed at a multiple of this frequency, and the LC orientation can be time-dependent as a consequence [31–33]. For the default setting of our SLM (so-called 22:6), the *addressing* rate is 120 Hz and allows the largest number of phase levels (q_{max}=256); this setting was used for the majority of measurements in this paper, unless stated otherwise. An alternative setting of the SLM (5:5) addresses the LC at 300 Hz

#103154 - $15.00 USD Received 23 Oct 2008; revised 27 Nov 2008; accepted 28 Nov 2008; published 3 Dec 2008

and has slightly fewer phase levels (q_{max}=192). Both the *refresh* rate and the *addressing* rate, and their overtones, modulate the intensity and the position of the laser beam, as can be seen in Fig. 5.

We have measured the amplitude of intensity modulation as a function of steering angle for a first-order beam on our optical table and found that for steering angles $\alpha_{norm} \leq 0.33$ (a larger range than used in our trap calibrations), the intensity fluctuates by less than $\pm 8\%$ of the average value for the 22:6 setting, while for the 5:5 setting, the intensity fluctuations are less than $\pm 2\%$ of the average value (data not shown). Thus, while these intensity modulations will affect the potential of the trapped particle, for the 5:5 setting they are smaller than the precision of our trap stiffness measurements (see below). The determinations of trap stiffness quoted in this work should be considered as average quantities determined over many SLM cycles.

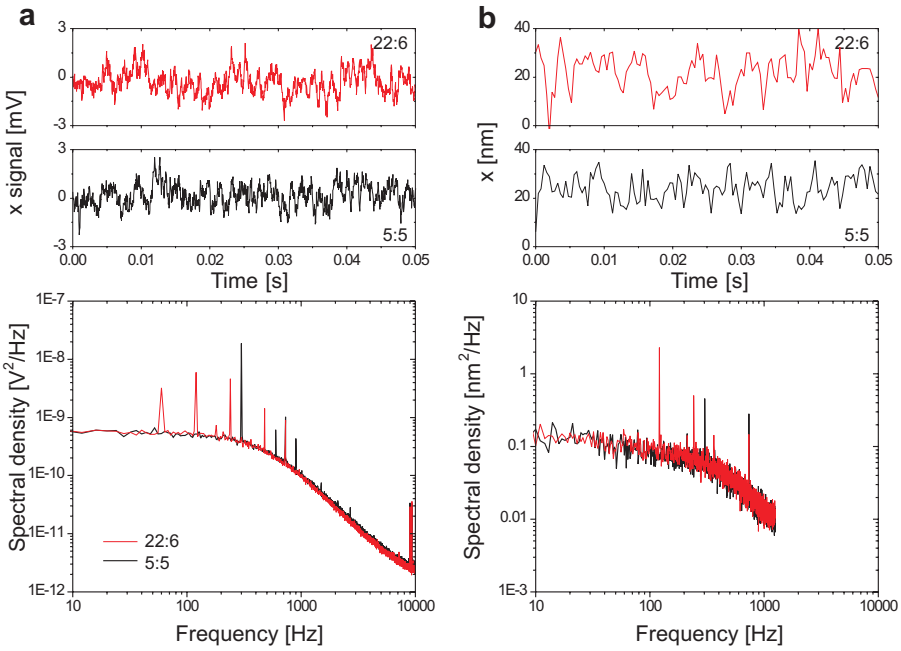

Fig. 6. (a) Laser deflection as a function of time, measured using the PSD, for 22:6 (top) and 5:5 (middle) SLM settings, and corresponding power spectra (bottom, average over 1000 spectra). A single particle was trapped in one of three HOT traps in the same configuration as in Fig. 9(a) with x=-9.9μm. (b) Position as a function of time for the same particle in the same configuration as in (a), determined from high-speed camera images (frame rate 2500 Hz), for 22:6 (top) and 5:5 (middle) SLM settings, and corresponding power spectra (bottom, average over 20 spectra). The laser power was 285 mW, measured before the focusing objective lens.

In PSD power spectra for a trapped particle (Figs. 4 and 6(a)), the temporal modulation of the beam is clearly visible. However, the PSD detects displacements of the particle relative to the laser light, and, depending on the position of the PSD along the optical axis, displacements of the laser trap itself. In addition, the light on the PSD includes all diffracted light that passes through both objectives. Hence, it is impossible to determine from PSD traces how much each optical traps position is modulated. To address this, we used our high-speed camera to capture

#103154 - $15.00 USD Received 23 Oct 2008; revised 27 Nov 2008; accepted 28 Nov 2008; published 3 Dec 2008

the trajectory of a trapped particle, which we then used for power spectrum analysis. From these camera-based power spectra (Fig. 6(b)), it is clear that the trap position is being modulated due to the SLM addressing. From the peaks in the spectra we estimate the extent of this position noise to be $\sim$5 nm for the 22:6 setting, and smaller for the 5:5 setting, a pointing instability of less than 2 μrad. The dependence of this noise on steering angle has not been thoroughly investigated and should be compared with the RMS displacement of the trapped particle in the optical potential in order to determine its relative importance to the measurement.

Having identified the peaks in our power spectra as intrinsic effects of the SLM, we proceed with experiments examining the fundamental operation and limitations of HOT technology for force measurements on biomaterials, namely the dependence of the (average) trap stiffness on steering angle and the accuracy with which a HOT trap (on average) can be positioned. Results presented here on trap stiffness measurements and trap displacements are determined from data recorded over times much longer than the 16.7 msec (60 Hz) refresh time of our SLM, and hence must be considered as time-averaged quantities for a given kinoform.

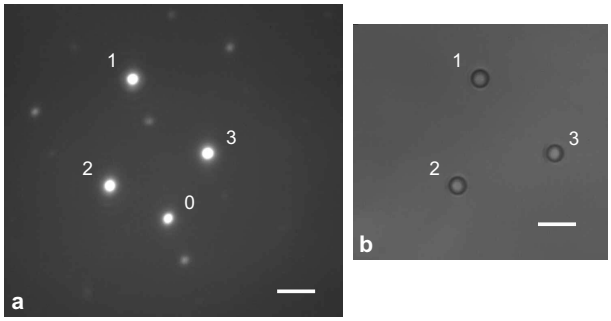

Fig. 7. (a) Trapping configuration used for several of our experiments, imaged by back-reflection of the laser foci from the coverslip. The brightest spots are three traps #1, #2, and #3 in a triangular configuration. Also visible are the zero-order spot and ghost traps due to higher-order interference. (b) Microscope image of three 2.1-μm-diameter particles trapped in the three HOT traps shown in (a). Scale bars in both images represent 5 μm.

4. Experimental results

4.1. Position dependence of κ

For each change in the position of one or more of the HOT traps, the entire kinoform sent to the SLM is changed. In this subsection we investigate how the stiffness of a trap changes when this trap is steered, or when it is stationary but another trap is steered. We used a configuration of three traps (Fig. 7), comparable to what one might use when probing biomaterials. The chosen configuration was asymmetric, to avoid having ghost traps overlap with desired traps [34]. We steered either one or two traps over a range of 3 to 4 μm, while the others were kept at fixed positions. By trapping a single particle in one of the traps we probed the stiffness of that trap in the *x* and *y* directions.

First, we moved only trap #2, in 7 steps of 0.52 μm directed away from trap #3, and then back to its original position in 14 steps of 0.26 μm. Figure 8(a) shows the trap stiffnesses κ_x (solid triangles) and κ_y (open triangles) for a particle in trap #1 for all these positions. In Fig. 8(b) the relative differences with respect to the mean value are given. By transferring the particle to trap #2, we probed the stiffnesses of trap #2 for the same positions of traps (Figs. 8(c) and 8(d)). The average stiffnesses of trap #1 (κ_x = 48 and κ_y = 50 pN/μm) were similar to those of trap #2 (κ_x = 47 and κ_y = 50 pN/μm). In both cases the trap stiffness was constant (within $\pm$ 4%)

#103154 - $15.00 USD Received 23 Oct 2008; revised 27 Nov 2008; accepted 28 Nov 2008; published 3 Dec 2008

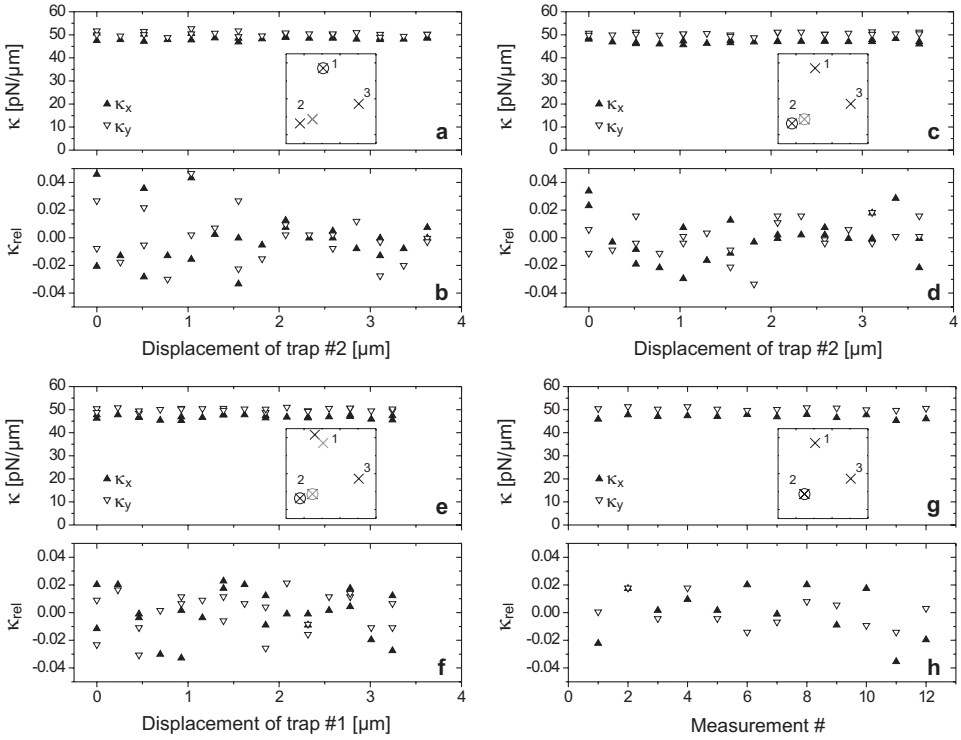

Fig. 8. Trap stiffness and relative difference with respect to the mean stiffness (κ_{rel} = (κ–$\langle\kappa\rangle$)/$\langle\kappa\rangle$) for several positions in a triangular configuration of traps (Fig. 7), for x (solid triangles) and y (open triangles). The laser power was 188 mW, measured before the focusing objective lens. (a-b) The stiffness of trap #1, while trap #2 was displaced. (c-d) Stiffness of trap #2, for the same displacements of trap #2 as in (a-b). (e-f) Stiffness of trap #2, while both trap #1 and trap #2 were displaced. (g-h) Stiffness of trap #2, while all traps were kept stationary. See text for details. Insets: position of the traps ($\times$) relative to each other and the range of motion of the displaced trap(s). The circle ($\otimes$) indicates which trap is probed with the trapped particle.

over the measured trap positions. At the positions that were revisited, the differences between first and second measurements were similar to the variation between different positions.

Next, while keeping the same particle in trap #2, we concurrently displaced both trap #1 and trap #2. The steps for trap #2 were the same as mentioned before; for trap #1 the step sizes were 0.47 μm (directed away from trap #3) and 0.23 μm (back to its original position). The results are shown in Figs. 8(e) and 8(f). Again, the trap stiffnesses varied within $\pm$ 3%, with κ_x = 47 and κ_y = 50 pN/μm.

To determine the accuracy of our method to measure the trap stiffness, we also obtained the stiffness for trap #2 twelve consecutive times, keeping the positions of all three traps fixed (Figs. 8(g) and 8(h)). The relative differences in stiffness were within $\pm$ 3% (κ_x = 47 and κ_y = 50 pN/μm). These results show that upon steering over μm-scale ranges, with different step sizes $\neq d_{2\pi}$, the trap stiffness remains constant within the resolution of this calibration method.

#103154 - $15.00 USD Received 23 Oct 2008; revised 27 Nov 2008; accepted 28 Nov 2008; published 3 Dec 2008

4.2. SLM efficiency

To investigate the range over which the trap stiffness remains constant, we again created three traps, of which two were held at fixed positions. A particle was trapped in the third trap, which was moved over large distances ($> 25\ \mu$m) in the *x*-direction (Figs. 9(a) and 9(b), laser power 286 mW) and *y*-direction (Figs. 9(c) and 9(d), 188 mW) and probed at steps of 1.65 μm. All positions were sampled twice. Over the measured range we found only a limited change in trap stiffness ($\pm$7%), both for κ_x (solid triangles) and for κ_y (open triangles), with a slight decrease in κ for larger distances.

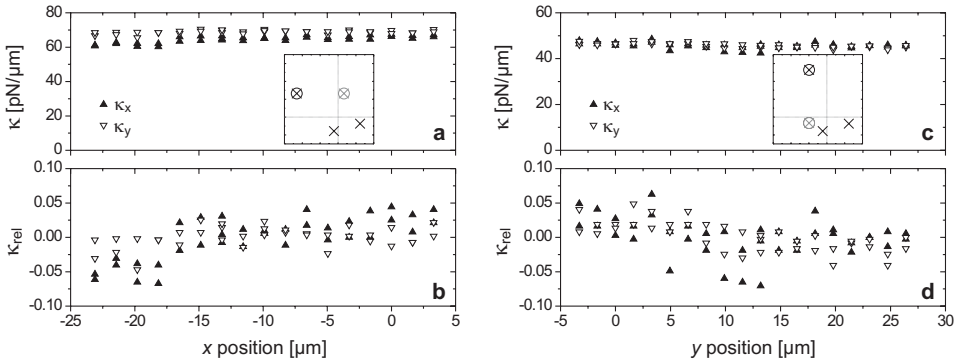

Fig. 9. Trap stiffness and relative difference with respect to the mean stiffness for *x* (solid triangles) and *y* (open triangles). Three traps were created of which one, holding the particle, was moved. (a-b) Trap moved in *x*-direction at y = 13.2 μm; laser power was 286 mW. (c-d) Trap moved in *y* at x = -9.9 μm; laser power was 188 mW. The *x* and *y* positions are with respect to the zero-order spot. Insets: position of the traps ($\times$) relative to each other and the range of motion of the displaced trap, with the circle ($\otimes$) indicating the probed trap.

In this experiment, the maximum distance over which the beam was steered away from the zero-order spot ($\sim$26 μm) corresponds to a normalized angle α_{norm} = 0.13 (Λ = 15 pixels). Comparing our trap stiffness results to the theoretical values for the efficiency η of the SLM to diffract power into the first-order beam (see Fig. 2 and Eq. (4)), we see that for α_{norm} = 0.13 the theoretical η is 98.5%. Our results similarly show a small decrease in stiffness, albeit more than predicted. However, the theory, which describes the efficiency due to pixelation and phase level quantization for a single, on-axis steered spot, does explain why we see only a limited decrease in our measurements, a result not found by others [19].

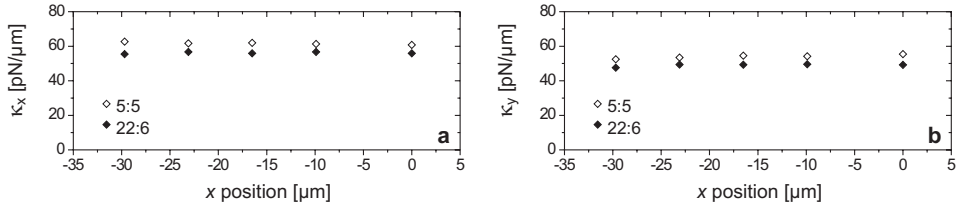

Fig. 10. Trap stiffnesses κ_x (a) and κ_y (b) for 5:5 (open diamonds) and 22:6 (solid diamonds) SLM settings. Three traps were created of which one, holding the particle, was moved. Trap configuration was the same as in Fig. 9(a); laser power was 286 mW. The *x* positions are with respect to the zero-order spot.

#103154 - $15.00 USD Received 23 Oct 2008; revised 27 Nov 2008; accepted 28 Nov 2008; published 3 Dec 2008

To test whether the independence of average trap stiffness on steering angle depended on SLM settings, we repeated these measurements at five trap positions over a range of 30 μm, for both the 22:6 and the 5:5 SLM settings (Fig. 10) using the same particle (though a different particle and sample cell than used in Fig. 9). The results in Fig. 10 demonstrate that the average trap stiffness does not change appreciably with steering angle for either SLM setting. However, it is apparent that the trap stiffness obtained using the 5:5 setting is systematically higher than that found with the 22:6 setting, a finding consistent with the lesser relaxation of LCs when using a faster address rate.

4.3. κ and laser power

Having established the range over which the trap stiffness κ is constant, we then looked at the achievable κ as a function of laser power in our HOTs, and at the fraction of power in the undiffracted zero-order spot.

We first trapped a particle in trap #2 of the triangular configuration of Fig. 7. We varied the laser power from 100 to 336 mW, and measured the trap stiffnesses κ_x (solid triangles) and κ_y (open triangles) (Fig. 11). We then moved the particle to the zero-order spot and measured the stiffness for the same power levels (up to 286 mW). We found a linear dependence of the stiffness on the laser power, in accordance with theory [1], both for the first-order trap #2 and for the zero-order spot. The linear fits (forced through zero) gave per 100 mW laser power for trap #2 κ_x = 25.4 pN/μm (solid line) and κ_y = 27.6 pN/μm (dashed line). For the zero-order spot, these values were κ_x = 11.1 pN/μm and κ_y = 11.3 pN/μm. Assuming all three HOT traps had equal stiffness, we find that the power in the zero-order spot was 14% of the total power in the three traps + zeroth order. We did not characterize the ghost traps, but from the image in Fig. 7(a) it can be seen that their intensity is far less than that of the zero-order spot.

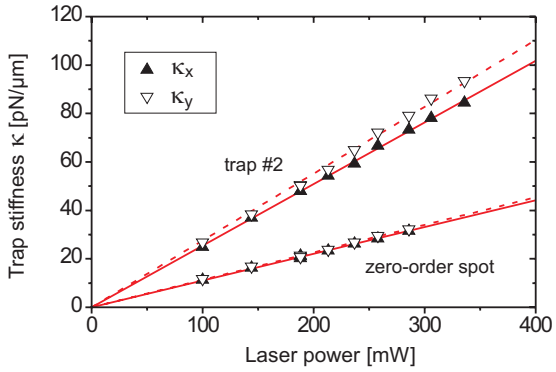

Fig. 11. Trap stiffnesses κ_x and κ_y as a function of laser power, for trap #2 and for the zero-order spot (see Fig. 7). Laser power is measured before entering the objective and ranges from 100 to 336 mW (#2) or to 286 mW (zeroth order). Linear fits are forced through zero.

From these results, we can estimate the maximum trap stiffness available for three traps in our HOT instrument. Our SLM is rated for a maximum input intensity of 2 W/cm^2. Because of overfilling the SLM and its efficiency, saturation would result in approximately 1 W directed towards the objective lens. At this power, the trap stiffness for three traps would be 250 pN/μm per trap, assuming a linear response beyond the range measured in Fig 11. These results indicate sufficiently high trap stiffnesses in multiple-trap configurations to probe soft materials [5], and

#103154 - $15.00 USD Received 23 Oct 2008; revised 27 Nov 2008; accepted 28 Nov 2008; published 3 Dec 2008

a relatively small loss of power into the zeroth order.

4.4. *Step resolution*

Since our setup has a large range over which we find an approximately constant κ, we investigated whether this meant sacrificing the position resolution of trap steering. As shown by Schmitz *et al.* [35], the theoretical minimum step size is significantly smaller than the step resulting from a 2π phase gradient step.

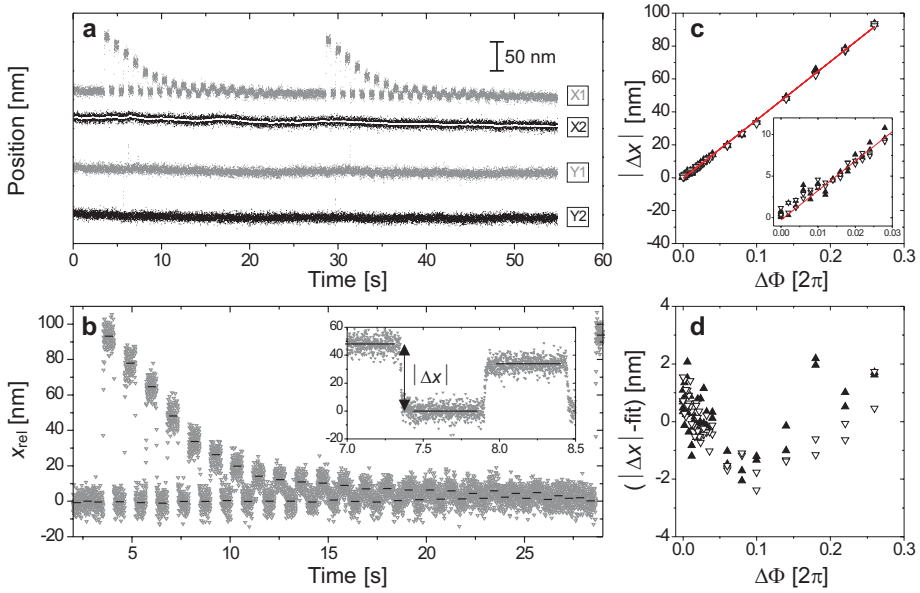

Fig. 12. (a) The x and y positions for trapped particles #1 (grey) and #2 (black), and the smoothed curve for x of #2 (white line). (Data are offset to fit in one graph and show positions from 68575 images recorded at 1250 fps.) (b) The x position of #1 corrected for drift using #2 (see text). The black lines show the average position over the indicated range. (c) Step size $|\Delta x|$ as a function of applied difference in phase shift $\Delta\phi$, for the first series (solid triangles) and for the second (open triangles). Inset: enlarged view. Linear fit (red line). (d) Difference between $|\Delta x|$ and the linear fit in (c). (For display purposes, (a) and the main graph in (b) only show 1 in every 5 data points.)

We created three traps separated by $\sim$9 μm in an asymmetric configuration, with laser power 560 mW, and captured 68575 images of two trapped particles at a rate of 1250 frames per second (55 seconds). With intervals of 0.54 s, we moved one of the traps in the x-direction and back to its original position, with decreasing step size $\Delta\phi$ varying from 0.52π to 0.004π (Fig. 12); this entire series of positions was done twice. The original position of the trap was offset by $x \approx 7.8$ μm ($\phi = 43.96$ π) and $y \approx 9.6$ μm ($\phi = 54.054$ π) from the zero-order spot. We used image correlation (see section 3.2) to determine the position of the particles in each image. To account for drift of the traps due to air currents or pointing stability of the laser, the smoothed curve (adjacent average over $\sim$0.2 s (241 points)) of the x-position of particle #2 was subtracted from the x-position of particle #1. The resulting curve is plotted in Fig. 12(b).

The HOT trap resided at each position for $\sim$675 frames. To ensure the dynamics of stepping were excluded [36], the average position of the particle was determined for the central

#103154 - $15.00 USD Received 23 Oct 2008; revised 27 Nov 2008; accepted 28 Nov 2008; published 3 Dec 2008

529 frames (indicated by the black lines in Fig. 12(b)). The absolute difference $|\Delta x|$ (see inset Fig. 12(b)) between each of these average positions is plotted in Fig. 12(c) as a function of the change in maximum phase retardation. The inset shows an expanded view of the small-step region ($\Delta\phi < 0.06\pi$). The slope of the linear fit (red line) gives the step size d per 2π phase retardation: $d_{2\pi}$ = 354 nm, which compares well to the theoretical value (Eq. (3)) for our setup of $d_{2\pi}$ = 369 nm (4% difference).

Differences between the observed step size and the linear fit (Fig. 12(d)) were within $\pm$ 2 nm for the measured range of $\Delta\phi$. Comparing the data for the first series (solid triangles) with the data for the second (open triangles), the error seems not to be random, but related to the position of the trap. The amplitude of this nonlinearity in positioning is comparable to the systematic positioning error that has been reported for AODs [37]. Assuming a linear response for the SLM allows positioning within $\pm$2 nm. If a higher resolution is required, the dependence of trap position on steering angle can be characterized to provide 1 nm position accuracy.

It must be emphasized that this position accuracy is of the time-averaged particle position in the trap. Underlying this time-averaged behavior is the modulation of trap position arising from LC modulation in the SLM (section 3.4), which can be comparable to this average positioning resolution. Thus, while an LC-based kinoform can position a trap within $\sim$2 nm of the desired position, the dynamics of the LC and limited addressing bandwidth [33] are at present the limiting factors of position stability in dynamic HOTs implemented with these SLMs.

5. Discussion and conclusions

To perform quantitative force measurements using optical traps, parameters such as trap stiffness and its position dependence, range of trap steering, minimum step size and trap stability are of key importance. In this work we investigated these features for our holographic optical tweezers.

We found, for a configuration of three HOT traps, a stiffness per trap of $\kappa \sim 26$ pN/μm per 100 mW of laser power, with a small amount of light (14%) remaining undiffracted in the zeroth order. The trap stiffness per trap was independent of the precise configuration of traps. Furthermore, when steering one or more of the traps, the stiffness stayed roughly constant over a range of tens of μm, independent of step size. For our setup, a limited change in trap intensity over this range was not unexpected, as a theory of the diffraction efficiency of the SLM due to pixelation and discrete phase levels [22, 23] predicts a decrease of $\sim$1.5%. Factors not considered in the theory used here, such as dead space and cross-talk between pixels, may be responsible for the larger decrease we observed. We have not investigated in detail what components of our system provide this relatively large range of constant trap stiffness compared with the range found by others [19, 20]. Nonetheless, we see from Sec. 2 that:

$$\frac{d}{\alpha_{norm}} = \frac{\lambda f_{obj}}{2ml_{pix}}, \tag{7}$$

which is the ratio that should be maximized to achieve the largest range of high efficiency by Eq. (4). The long wavelength λ, long focal length of our objective lens f_{obj}, and small pixel pitch l_{pix} of our SLM all contribute to this large range. A larger SLM with the same (or smaller) pixel pitch would further increase this range, as it would require $m<1$ for reimaging onto the back aperture of the objective lens.

The calibrations performed here involved analyzing the power spectrum of laser deflections from a trapped particle. The use of a single particle in a multiple-trap configuration enabled the use of a photodiode for high-bandwidth position detection. The independence of trap stiffness on position demonstrated with this high-throughput approach means that it is not necessary to calibrate the trap stiffness separately for each desired trap position used in a dynamic measure-

#103154 - $15.00 USD Received 23 Oct 2008; revised 27 Nov 2008; accepted 28 Nov 2008; published 3 Dec 2008

ment. Instead, power spectral determination, e.g. from high-speed camera imaging of multiple trapped particles, need only be performed once to obtain the stiffness for each trap that will be used in subsequent manipulation experiments.

For future experiments investigating the depth dependence of trap stiffness, the use of a water-immersion objective lens is preferred, as it overcomes problems of spherical aberration [20]. The extension of trapping and calibration to the third dimension can be accomplished using kinoforms that include lensing [12] and 3D position detection using laser-based techniques [38] or holographic particle imaging [39]. Future experiments taking advantage of high-speed imaging can also be used to investigate the effect of the pulsed modulation of electrically addressed SLMs on the particle dynamics. Furthermore, by applying flow to the trapped particles, the shape of each trapping potential and the range of displacements over which a linear restoring force applies can be determined [19].

In addition to the stiffness measurements, we investigated whether our large value of d/α_{norm} $\approx 200\mu$m limited the step size of the HOT traps. We found that we can control and detect the average position of the traps to $\sim$2 nm. However, there is a temporal modulation of the trap position due to SLM addressing, which we estimate to be of the same order for the more stable setting of our SLM. This nanometer-scale positioning accuracy and position stability are sufficient for many force-measurement applications.

Our measurements have demonstrated that trap stiffness is constant and high over a wide range of beam steering angles in our HOT instrument, and furthermore that traps can be steered in step increments as small as 1 nm. These results demonstrate that this technique is capable of quantitative force measurements. The disadvantages of this technique over alternative methods of beam steering, such as AODs, are the slower update bandwidth and lower temporal stability of optical traps, although AODs have their own limitations of position accuracy [37]. Applying HOTs to force measurements on biomaterials has distinct advantages over other techniques, since the traps are "always on" (as opposed to time-shared), and traps can be located and steered in all three dimensions within the sample. In conclusion, the accurate steering of HOT traps and the independence of their stiffness over a wide range of positions demonstrates that HOTs can be used in quantitative force measurements on soft biomaterials.

Acknowledgments

This work has been funded by the Canada Foundation for Innovation (CFI) and the Natural Sciences and Engineering Research Council of Canada (NSERC). NRF is a Scholar of the Michael Smith Foundation for Health Research and a Cottrell Scholar of the Research Corporation. We thank Daniel Burnham for use of his LabVIEW code for SLM control [24], and Jennifer Curtis, Raghuveer Parthasarathy and John Bechhoefer for discussion and critical reading of the manuscript. We are particularly grateful to an anonymous reviewer for stimulating further investigation of the SLM peaks observed in our power spectra.

#103154 - $15.00 USD Received 23 Oct 2008; revised 27 Nov 2008; accepted 28 Nov 2008; published 3 Dec 2008